Experimental and numerical investigations on deformation of cylindrical shell panels to underwater explosion

K. Ramajeyathilagam[a], C.P. Vendhan[b,*] and V. Bhujanga Rao[a]
[a]*Shock and Vibration Center, Naval Science and Technological Laboratory, Visakhapatnam 530027, India*
[b]*Ocean Engineering Department, Indian Institute of Technology Madras, Chennai, 600036, India*

Received 5 May 2000
Revised 24 April 2001

Experimental and numerical investigations on cylindrical shell panels subjected to underwater explosion loading are presented. Experiments were conducted on panels of size $0.8 \times 0.6 \times 0.00314$ m and shell rise-to-span ratios $h/l = 0.0, 0.05, 0.1$, using a box model set-up under air backed conditions in a shock tank. Small charges of PEK I explosive were employed. The plastic deformation of the panels was measured for three loading conditions. Finite element analysis was carried out using the CSA/GENSA [DYNA3D] software to predict the plastic deformation for various loading conditions. The analysis included material and geometric non-linearities, with strain rate effects incorporated based on the Cowper-Symonds relation. The numerical results for plastic deformation are compared with those from experiments.

1. Introduction

Non-contact underwater explosions are widely used to cause damage to ship structures as a part of naval warfare strategy. The response of structures subjected to the resultant shock loading is quite complex involving fluid – structure interaction, high strain rates, material and geometric non-linearities, large deformation, tensile tearing and rupture. Depending on the explosion energy, the structural response is either elastic or plastic. The sequence of failures associated with underwater explosion is elastic deformation, large deformation, tensile tearing, shear failure etc. Keil [1,2] has briefly dealt about underwater explosion, failure and damage mechanisms. A number of investigations on stiffened and unstiffened plates and beams subjected to air blast loading [3–18] have been reported in the literature. There does not appear to be any published work dealing with underwater explosion effects on cylindrical panels.

Menkes and Opat [18] reported three failure modes, namely, a) large deformation, b) tensile tearing and c) shear failure for explosively loaded clamped beams. Similar failure modes have been found in the case of unstiffened and stiffened plates to air blast loading [11, 12]. Ramajeyathilagam et al. [19] have also established the first two failure modes for rectangular plates under air backed condition subjected to underwater explosion on the basis of shock tank tests and numerical analysis.

Cylindrical shell panels find wide use in ship and offshore structures and hence there is a need to understand their behavior under shock loading. In the present paper an experimental investigation on the large deformation of cylindrical shell panels subjected to underwater explosion is presented followed by numerical modelling. The experiments were carried out on air-backed cylindrical shell panels with rise-to-span ratio $h/l = (0.0, 0.05, 0.1)$, to study the curvature effects on the shock response. The experiments were conducted using small explosive charges of PEK I in a shock tank. Numerical analysis has been carried out using the CSA/GENSA [DYNA3D] [20] non-linear finite element code and the results compared with experimental data.

2. Experimental work

Experiments were conducted in a shock tank of dimensions $15 \times 12 \times 10$ (depth) m. The test fixture used

*Corresponding author: Fax: +91 044 2350509; E-mail: vendhan@iitm.ac.in.

Shock and Vibration 8 (2001) 253–270
ISSN 1070-9622 / $8.00

to study the large deformation behavior of curved shell panels is shown in Fig. 1. The test set-up consists of a heavy steel box to simulate air- backed condition, a top hollow cover plate and two end plates, which have been machined to match the curvature of the test panels corresponding to $h/l = 0.05$ and 0.1. All the fixture plates were made of 0.025 m thick mild steel plates.

The test panels were fabricated from cold rolled high strength, low alloy, mild steel plates of dimensions $0.8 \times 0.6 \times 0.00314$ m. The cylindrical panels were formed by setting the required radius on a plate bending machine. A typical shell panel is shown in Fig. 2. The exposed (base) area of the panel to shock loading is $0.6 \times 0.4\,\mathrm{m}^2$, with the load acting on the convex side. The experiments were carried out using small explosive charges of PEK I (1.17* TNT) of 20 gm, 30 gm and 50 gm weights. The explosive was packed in a small spherical plastic container, appropriately designed for each charge weight, and detonated electronically. In the experimental set-up, the test panel was placed between the bottom box and the top cover plate. End plates matching the curvature were used at the curved ends to prevent water entering the box. The complete set-up was bolted using 30 M12 bolts along the edges with 0.1 m of the test panel held between the fixture plates.

The test fixture along with the test panel was immersed in the shock tank (at the NSTL, Visakhapatnam) to a water depth of 2.0 m to eliminate the effect of surface reflections on the panel during early response. The side walls and the bottom of the tank remained at 6 m and 8 m, respectively, away from the explosion. Hence, the influence of reflections from the bottom and side walls on the early response is considered negligible. The explosive charge was attached at a known distance by the use of a channel section fixed to the box model (see Fig. 1). In all the experiments, the explosive was placed on the normal line passing through the center of the panel at a stand-off distance of 0.2 m, measured from the base of the panel.

The permanent deformation of the panel was measured after each test, with the test panels secured to the fixture, as follows: Grids were marked before each test on a quadrant of the test panel corresponding to the finite element mesh, employed in the numerical analysis. Also markings were made on the top cover plate to match with the grid lines. A thin rectangular beam was placed over the curved top cover plate at each grid line, one after another. The depth of dishing was measured from the top of the beam with the help of a vernier. Subsequently the final deformation of the panel was obtained by deducting the depth of the beam and the thickness of the curved top cover plate from the originally measured displacement.

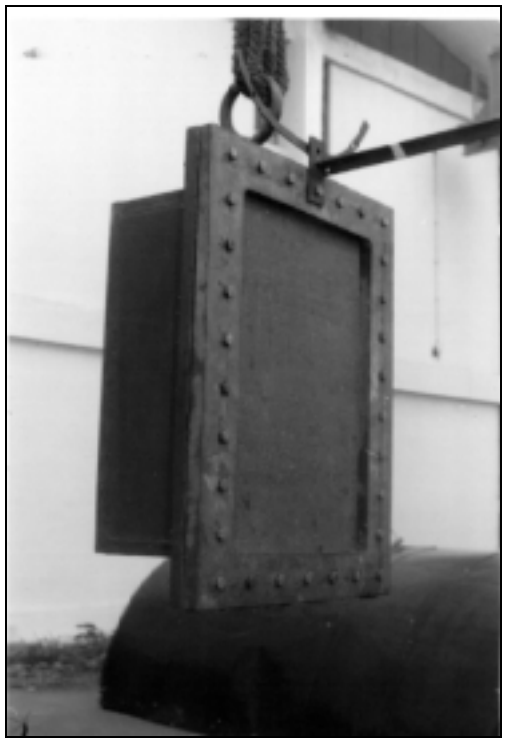

Fig. 1. Panel test fixture.

3. Finite element analysis

3.1. Finite element formulation

The finite element analysis of the test panel was performed using CSA/GENSA [20], a commercially available version of the DYNA3D non-linear finite element analysis software. Hughes-Liu shell elements [21] available in the GENSA code were employed for modelling the test panel. In the above code, the material non-linearities are modeled by the Von- Mises yield criterion and its associated flow rule with a bilinear stress – strain law. The geometric non-linearities are based on large deformation finite strain formulation. The finite element equations of motions for the assemblage of elements, derived based on the principle of virtual work, may be written in the form [20]

$$[M]\{\ddot{X}\} = \{P\} - \{F\} + \{H\} \tag{1}$$

where $[M]$ denotes the diagonal mass matrix, $\{P\}$ the sum of external and body force vectors, $\{F\}$ the stress

Table 1
Maximum shock pressure at the center of the plate (standoff distance = 0.2 m)

S. No.	Test No.	Shell rise ratio (h/l)	Charge weight ($\times 10^{-3}$ kg)	Effective standoff distance (m)	Shock factor ($0.45 \times W^{1/2}/R$) ($kg^{1/2}/m$)	Peak pressure (MPa)
1	HL001	0.00	20	0.2	0.318	156.0
2	HL002	0.00	30	0.2	0.390	181.0
3	HL003	0.00	50	0.2	0.503	220.0
4	HL051	0.05	20	0.18	0.354	175.0
5	HL052	0.05	30	0.18	0.433	204.0
6	HL053	0.05	50	0.18	0.559	247.0
7	HL11	0.10	20	0.16	0.398	199.0
8	HL12	0.10	30	0.16	0.487	232.0
9	HL13	0.10	50	0.16	0.629	282.0

divergence vector and $\{H\}$ the hourglass resistance. The stress divergence vector and hourglass resistance vector are given by [20]

$$\{F\} = \int_v [B]^T \{\sigma\} dv \tag{2}$$

$$\{H\} = -a_n \sum_j h_{ij} r_{jk} \ (i = 1, 3) \tag{3}$$

where,

$$h_{ij} = \sum_k V_i^k r_{jk} \tag{4}$$

and

$$a_n = Q_{ng} \rho v_e^{2/3} c/4 \tag{5}$$

Here $[B]$ is the strain -displacement matrix (with t denoting the transpose), $\{\sigma\}$ the stress vector, r_{jk} the hourglass base vector, h_{ij} the magnitude of hourglass mode, v the element volume, c the sound speed in the material, Q_{ng} a constant with value between 0.05 and 0.15 and V_i^k the nodal velocity of the kth node in the ith direction. The set of non-linear equations given in Eq. (1) are solved using the central difference scheme.

3.2. Modeling of the test panels

Considering the experimental fixing conditions with 0.025 m thick plates, the 0.00314 m thick test panel was assumed to be fixed at the edges of the exposed area (0.6×0.4 m^2); i.e. the three displacements and two bending slopes were assumed to be zero at the edges. Because of symmetry in loading and structure, only one quadrant of the exposed area (i.e. 0.3×0.2 m^2) of the test panel was considered for the analysis. The Hughes-Liu shell element was selected to model the test panel because of its robustness and greater accuracy when encountering finite strain [20]. The quarter panel was modeled using two grid sizes of 10×10 and 20×20 elements for some representative cases. Both the meshes converged to virtually the same results. Therefore, for all the subsequent analysis, the mesh of lower density (10×10 grid) as shown in Fig. 3 was used to achieve computational economy.

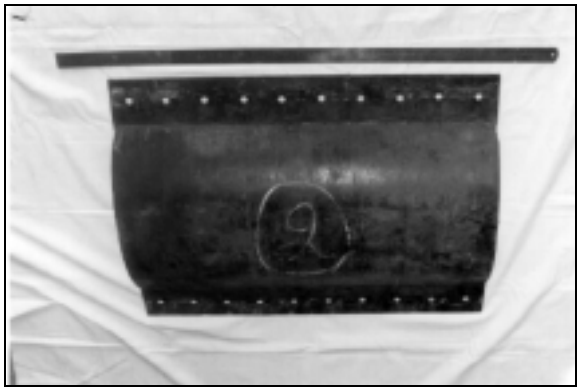

Fig. 2. Typical test panel ($h/l = 0.1$).

3.3. Material model

The uniaxial stress strain properties obtained for high strength, low alloy, mild steel have been used as the primary material data:

Elastic modulus	$E = 2.1 * 10^5$ MPa
Poisson's ratio	$\gamma = 0.3$
Mass density	$\rho = 7860.0$ kg/m^3
Tangent modulus	$Et = 250.0$ MPa
Static yield stress	$\sigma_y = 400.0$ MPa
Rupture strain	$\varepsilon_{\mathrm{rup}} = 0.23$

The constitutive model selected for the non-linear analysis of the panels using the GENSA code is the elasto – plastic material model with isotropic hardening. In order to include the effect of strain rate in the finite element analysis, the elasto-plastic analysis has been first carried out ignoring this effect, i.e. the static

Table 2
Permanent central deflection from experiments

S. No.	Test No.	Shell rise ratio (h/l)	Charge weight ($\times 10^{-3}$ kg)	Effective standoff distance (m)	Shock factor ($0.45 \times W^{1/2}/R$) ($kg^{1/2}/m$)	Permanent deformation (m)**
1	HL001	0.00	20	0.2	0.318	0.0446
2	HL002	0.00	30	0.2	0.390	0.0554
3	HL003	0.00	50	0.2	0.503	0.0736
4	HL051	0.05	20	0.18	0.354	0.0687
5	HL052	0.05	30	0.18	0.433	0.0816
6	HL053	0.05	50	0.18	0.559	0.1079
7	HL11	0.10	20	0.16	0.398	0.0854
8	HL12	0.10	30	0.16	0.487	0.0988
9	HL13	0.10	50	0.16	0.629	0.1247

**Measured positive towards the base from the top.

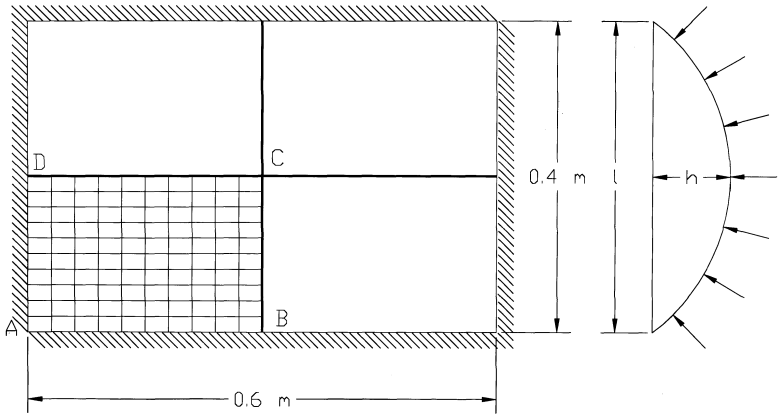

Fig. 3. Finite element modelling of the shell panel.

yield stress has been employed in the analysis. The average strain rate has been calculated from the maximum effective plastic strain curve obtained from the analysis. The effective platic strain $\left(\varepsilon^p_{eff}\right)$ is given by [20]

$$\varepsilon^p_{eff} = \int_0^t \left(\frac{2}{3}\dot{\varepsilon}^p_{ij}\dot{\varepsilon}^p_{ij}\right)^{1/2} dt \tag{6}$$

where the plastic strain rate is given by the difference between the total strain rate $(\dot{\varepsilon}_{ij})$ and elastic strain rate $(\dot{\varepsilon}^e_{ij})$ as

$$\dot{\varepsilon}^p_{ij} = \dot{\varepsilon}_{ij} - \dot{\varepsilon}^e_{ij} \tag{7}$$

Subsequently, the dynamic plastic effects on the deformation of the panel have been incorporated by adjusting the dynamic yield stress (σ_{dy}) using the Cowper – Symonds relation [22] given by

$$\sigma_{dy} = \sigma_y \left(1 + \left|\frac{\dot{\varepsilon}}{D}\right|^{\frac{1}{n}}\right) \tag{8}$$

where σ_y is the static yield stress and D and n are other material parameters, and for the strain rate $\dot{\varepsilon}$, which strictly speaking is a function of time, the average value mentioned above has been employed. In the present calculations, $D = 40/\text{sec}$ and $n = 5$ [10], being the commonly accepted values for mild steel, have been used. Thermal effects were not included in the analysis.

3.4. Shock pressure loading

The empirical pressure time history at any location with an instantaneous pressure increase followed by a decay, approximated by an exponential function, is given by [23]

$$P(t) = P_0 e^{-(t-t_d)/\theta} \quad 0 \leqslant t \leqslant \theta \tag{9}$$

For trinitrotoluene (TNT), the peak pressure (P_0) and the decay constant (θ) are given by

$$P_0 = 52.16 * 10^6 \left(\frac{W^{1/3}}{R}\right)^{1.13} \tag{10}$$

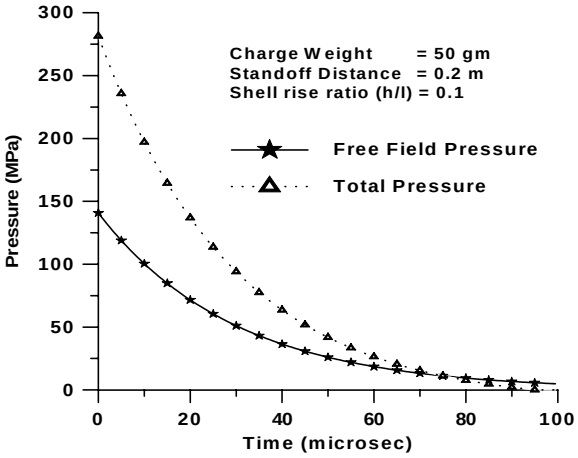

Fig. 4. Typical pressure time history at the center of the panel.

$$\theta = 92.5 * W^{1/3} \left(\frac{W^{1/3}}{R}\right)^{-0.22} \tag{11}$$

where $P(t)$ is the pressure (Pa) at any instant of time t, P_0 the peak pressure of the shock front, θ the decay constant (μsec), t the time variable (μsec), W the charge weight (kg), $t_d = (R - R_0)/c$ the time delay (μsec), R the stand off distance (m), R_0 the shortest radial distance and c the sound speed in water (m/sec).

When the free field pressure given in Eq. (9) impinges on the panel, it undergoes diffraction and scattering and hence the net pressure loading on the curved panel is modified by the interaction between the fluid and the structure. For an infinite plate submerged in water, Taylor's plate theory [24] provides the resultant over pressure accounting for the fluid-structure interaction effect. In the present study this theory is assumed to be valid for finite curved panels also. Thus, based on Taylor's plate theory the total pressure on the panel considering fluid – structure interaction is given by

$$P_t = 2 * P(t) - (\rho c v(t)/\sin\phi) \tag{12}$$

where

$$v(t) = \frac{2P_0}{\rho c}\frac{1}{z-1}\left\{e^{t/z\theta} - e^{t/\theta}\right\} \tag{13}$$

$$z = \frac{m}{\rho c \theta} \tag{14}$$

$$\phi = \sin^{-1}(R_0/R) \tag{15}$$

Here, P_t is the total pressure (Pa) on the plate at time t, ρ the fluid density (kg/m^3), m the mass per unit area, z the characteristic mass ratio, $v(t)$ the plate velocity (m/sec) and ϕ the angle of attack of the shock wave. It is noted that the shock wave propagation in the above theory uses the plane wave acoustic approximation. For the purpose of non-linear finite element analysis, the pressure on each finite element is computed using Eq. (12) at the center of the element. A spherical spreading assumption has been used to approximate the pressure variation over the panel. A typical pressure

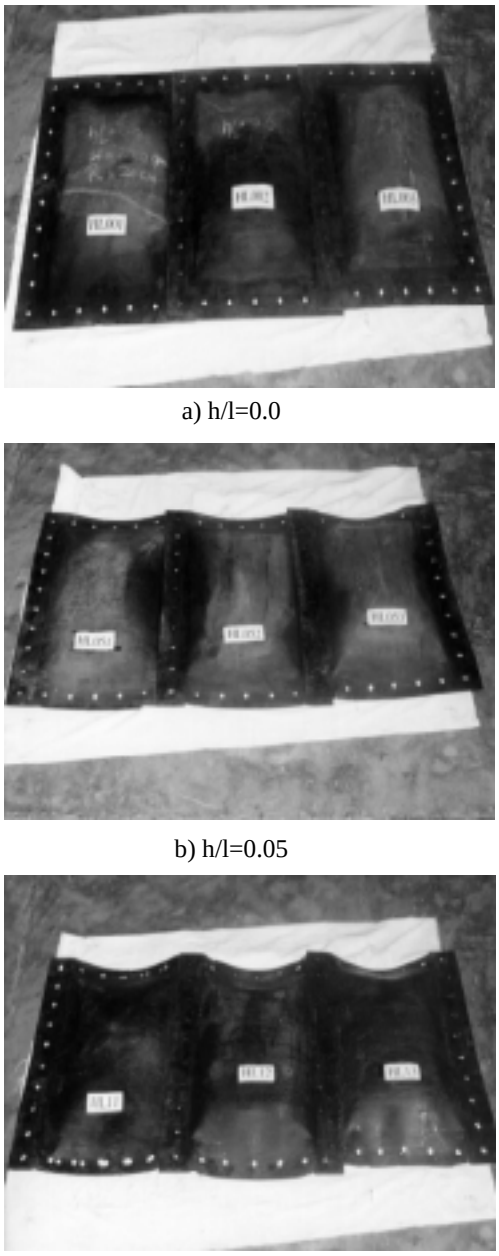

a) h/l=0.0

b) h/l=0.05

c) h/l=0.1

Fig. 5. Dishing of shell panels (3 in each category, see Table 1) (Panels shown concave up).

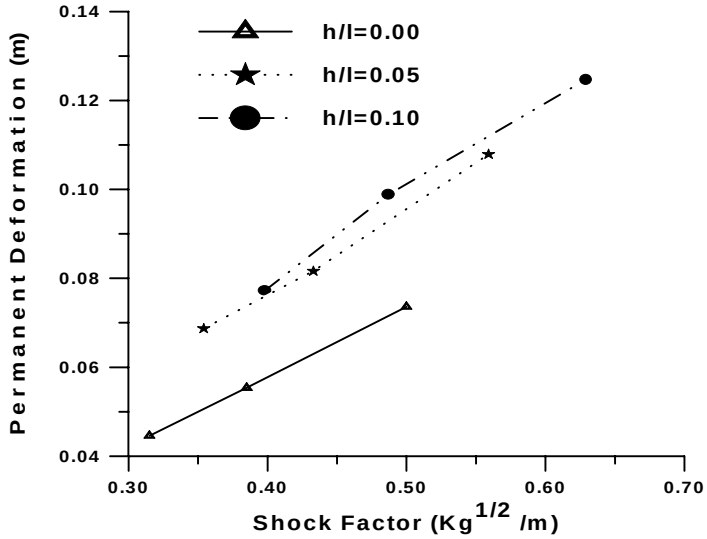

Fig. 7. Shock factor Vs permanent deformation (Experimental).

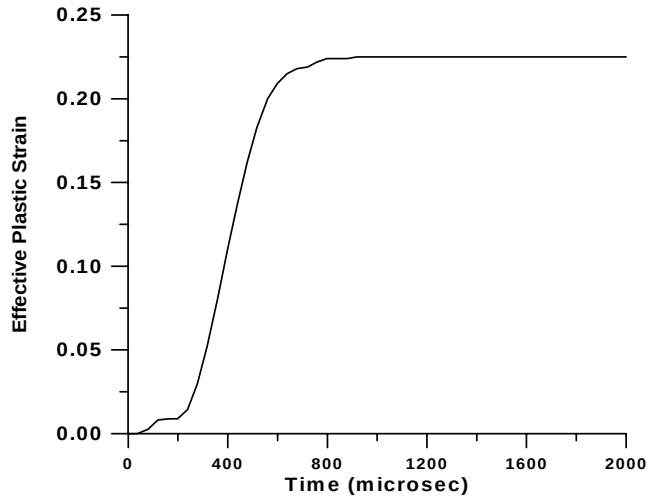

Fig. 8. Typical effective plastic strain time history (Numerical).

time history (both total and free field using Eqs (9) and (12) at the center of the panel (with $h/l = 0.1$) corresponding to a 50 gm charge weight at 0.2 m standoff is shown in Fig. 4. The peak pressure estimated for the various test conditions at the center of the panel are given in Table 1.

4. Results and discussions

4.1. Experimental

The permanent central deflection of the shell panels, measured positive from the panel towards the base (i.e. deflections normal to the base) for various loading conditions are presented in Table 2. The 'dished' shell panels are shown in Fig. 5. The permanent deformation of the shell panels measured from the original position along the longitudinal and transverse center lines (DC and BC in Fig. 3) are shown in Fig. 6. Although the deformation pattern for $h/l = 0.05$ and 0.1 are somewhat similar to that of the flat panel (i.e. $h/l = 0.0$), it is essential to note that the shallow shell configuration undergoes snap through. For computing the shock factor ($SF = 0.45 * W^{1/2}/R$; W the charge weight (kg), R the effective standoff distance (m)), the effective standoff distance is taken to be $R =$ (standoff distance from

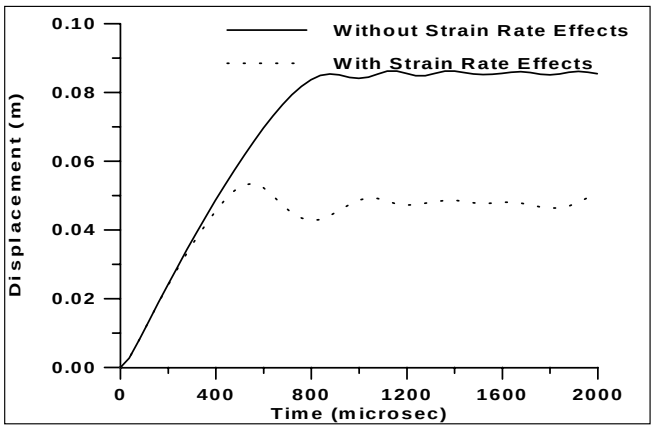

a)SF = 0.318

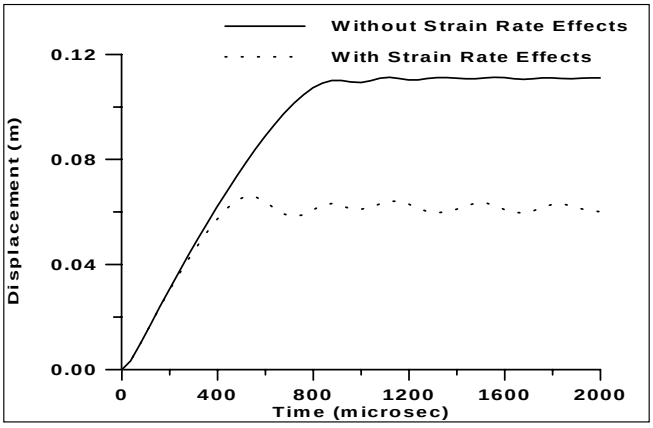

b) SF = 0.390

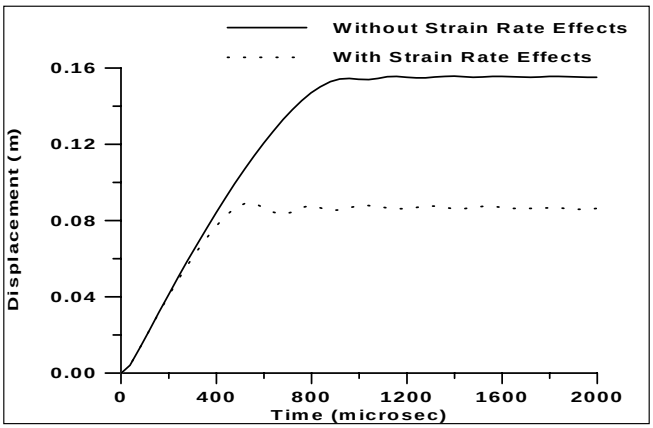

c) SF =0.503

Fig. 9. Displacement time history for $h/l = 0.0$ (Numerical).

the base – the shell rise at the center). SF Vs the maximum permanent deformation (at the center, point C in Fig. 3) for various shell panels is plotted in Fig. 7. The permanent deformation of the panel evidently increases with increase in the shock load. It is interesting to note that the permanent set increases with rise ratio (for the

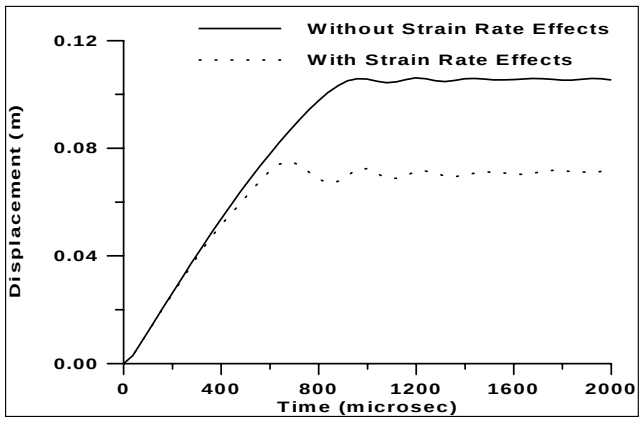

a) SF =0.354

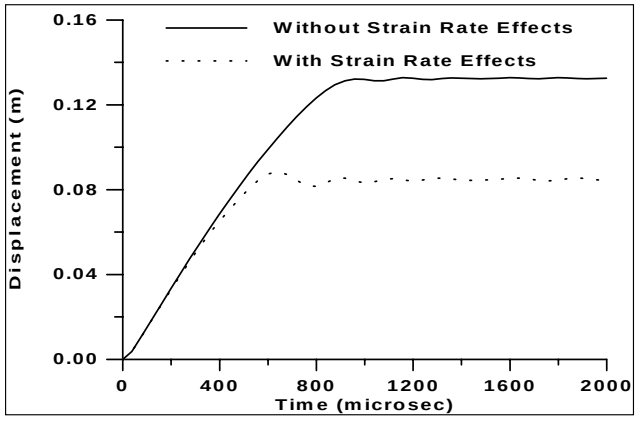

b) SF = 0.433

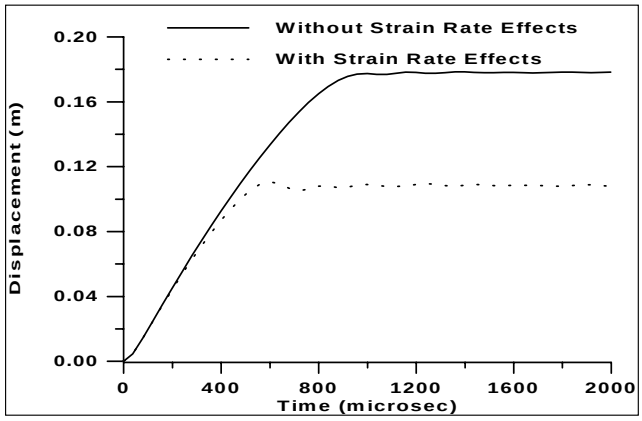

c) SF =0.559

Fig. 10. Displacement time history for $h/l = 0.05$ (Numerical).

two cases tested), which may be ascribed to the snap through behavior. All the experiments were aimed at causing mode I failure and in none of the experiments tensile tearing was observed.

4.2. Numerical

The numerical analysis for all the test conditions have been carried out using the CSA/GENSA

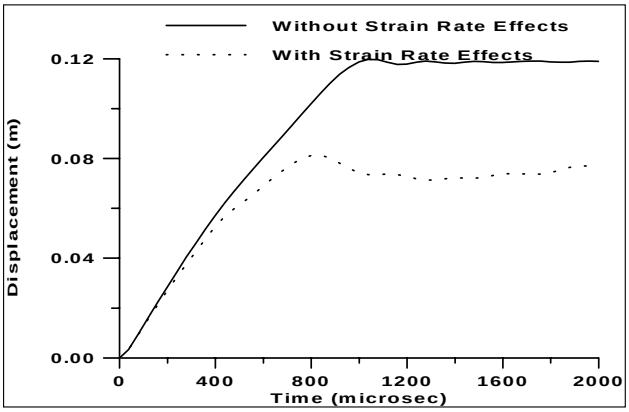

a) SF =0.398

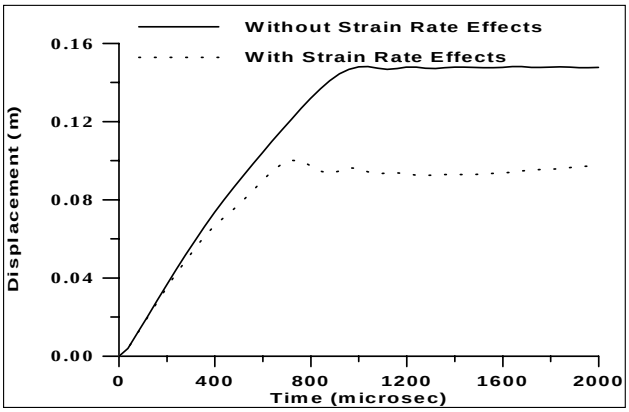

b) SF =0.487

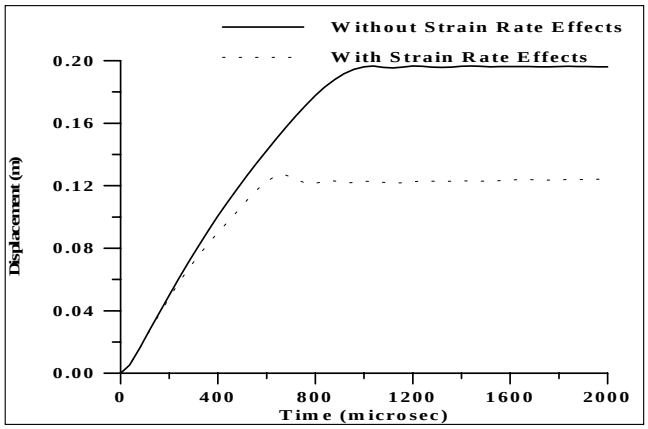

c) SF =0.629

Fig. 11. Displacement time history for $h/l = 0.1$ (Numerical).

[DYNA3D] explicit integration code. Because the method employed is conditionally stable, the choice of time step is very important in the analysis. Three different incremental time steps were used to study the numerical convergence for a typical case. The selected time steps of 0.5 μsec, 1.0 μsec and 2.0 μsec were found to meet the stability requirements of the explicit integration scheme. Since the results for the three time

Table 3
Strain rate and dynamic yield stress

S. No.	Test No.	Shell rise ratio (h/l)	Shock factor	Strain rate (1/sec)	Dynamic yield stress (MPa)**	Yield stress factor*
1	HL001	0.00	0.318	504.0	1064.0	2.66
2	HL002	0.00	0.390	832.0	1134.0	2.835
3	HL003	0.00	0.503	1071.0	1172.0	2.93
4	HL051	0.05	0.354	281.6	991.0	2.478
5	HL052	0.05	0.433	520.0	1068.0	2.67
6	HL053	0.05	0.559	1023.0	1165.0	2.913
7	HL11	0.10	0.398	176.0	938.0	2.345
8	HL12	0.10	0.487	460.0	1052.0	2.63
9	HL13	0.10	0.629	772.0	1123.0	2.801

*Yield stress factor = Dynamic yield stress/ Static yield stress.
**Static yield stress = 400 MPa.

steps did not differ much, 1.0 μsec time step was selected for subsequent analysis.

The analysis has been performed first without strain rate effects and with strain rate effects later, by adjusting the dynamic yield stress in the analysis based on the Cowper – Symonds relation as discussed earlier. The average strain rate has been obtained from the effective plastic strain time history curve obtained from the numerical analysis. The maximum effective plastic strain time history for the shell panel ($h/l = 0.05$) corresponding to a charge weight of 20 gm is shown in Fig. 8. The effective plastic strain is found to increase until about 800 μsec and then reach a plateau. The average strain rate used for the analysis has been computed from the maximum plastic strain and the time taken to reach the maximum.

The displacement time history for various loading conditions for $h/l = (0.0, 0.05, 0.1)$ is shown in Figs 9–11. From the curves it can be seen that the displacement time history at the center of the panel shows a nearly linear trend upto the maximum and found to have small oscillations thereafter as reported in other studies [11,12,20]. This means that most of the kinetic energy imparted to the panel by the shock loading has been dissipated as plastic work. As a result, the difference between the maximum displacement and the permanent deformation was quite small.

It is also observed from the curves that the total displacement and the permanent deformation decrease by about 44% for flat panels and 36% for curved panels because of strain rate effects. The time of occurrence of the maximum displacement was reduced considerably (see Figs 9–11) when the strain rate effects were introduced. The reduction in the permanent deformation and the occurrence of the maximum displacement are similar to that reported for plates subjected to air blast [10] or underwater shock [19].

The strain rate and the corresponding dynamic yield stress based on the numerical analysis are presented in Table 3. The average strain rate varies considerably so does the dynamic yield stress (Fig. 12) similar to that reported for plates by Olson et al. [10] under air blast loading and Ramajeyathilagam et al. [19], for underwater shock. The yield stress factor (dynamic yield stress / static yield stress) is found to vary between 2 and 3 for the test cases considered. At this juncture, it may be noted that because the stand-off distance was kept at 0.2 m in all the tests, the three test panels experienced different pressure loading, with the intensity increasing with the rise ratio. In spite of this, the strain rate is found to be less for the curved panels compared to the flat plate, which may be ascribed to the shell membrane effects. Also it is noted that smaller dynamic yield stresses associated with reduced strain rates for the curved panel may also be partly responsible for the higher permanent set in the case of curved panels compared to a flat plate (see Fig. 7). The influence of geometric imperfections as well as residual stresses that might have been caused due to fabrication of the shell panels, could not be investigated.

4.3. Comparisons

The central permanent deformations obtained from experiments and numerical analysis, with and without strain rate effects, are compared in Fig. 13. The numerical results show the same trend as the experimental results, namely increase in permanent set with both shock factor and shell rise ratio. It is seen that the computed permanent set values without strain rate effect are about 55% to 65% more than that of experimental values. The numerical model using average strain rate effects predicts values close to the experimental values within 10% accuracy. The measured and computed

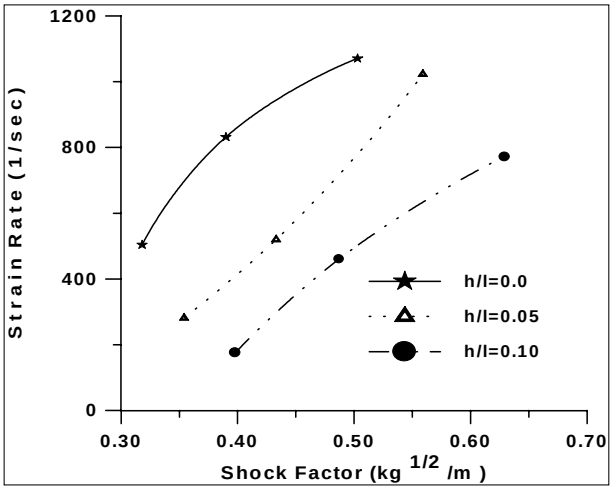

a) Shock factor Vs Strain rate

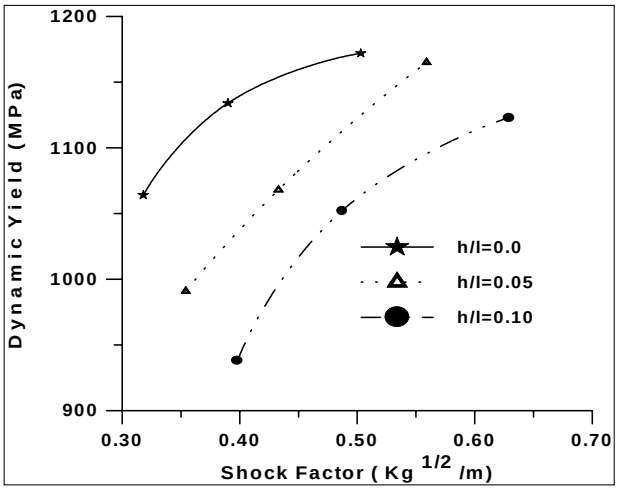

b) Shock factor Vs Dynamic yield

Fig. 12. Strain rate and dynamic yield stress.

permanent deformations of the panels (with strain rate effects) along the center lines (DC and BC in Fig. 3) are compared in Figs 14–16. The numerical prediction was found to be lower than the experimental values near the edges and crossed to the other side roughly at a distance of one fourth length of the panel for the flat plate. In the center of the panel, the predicted permanent deformation was found to be on the higher side compared to the experimental values. This trend for the flat panel is similar to that reported for square plates [10]. For the cylindrical shell panels, the crossing over has progressed towards the center of the panel (Figs 15 and 16). The comparison of permanent deformation pattern over a quadrant for a typical test panel ($h/l = 0.1$) corresponding to a charge weight of 30 gm is shown in Fig. 17. Overall, numerically predicted deformation shows a reasonable correlation with that of experiments, the comparison being better in the central region. The numerical analysis is not able to predict the permanent set near the edges accurately because of the plastic hinge formed near the edges, which could not be considered in the numerical model.

5. Conclusions

The results of the experimental and numerical investigations carried out on cylindrical shell panels ($h/l = 0.0, 0.05, 0.1$) subjected to underwater explosion are presented. The numerical study shows that the

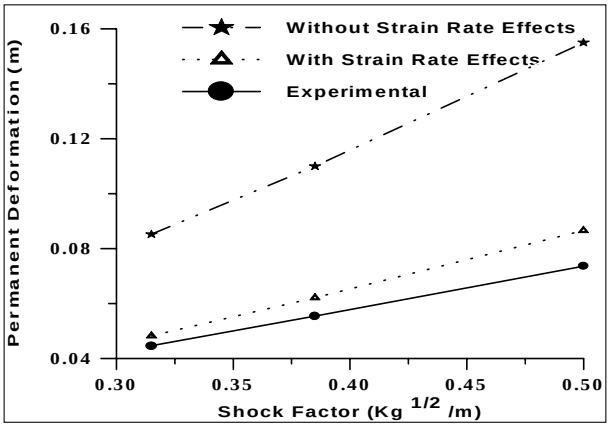

a) h/l=0.00

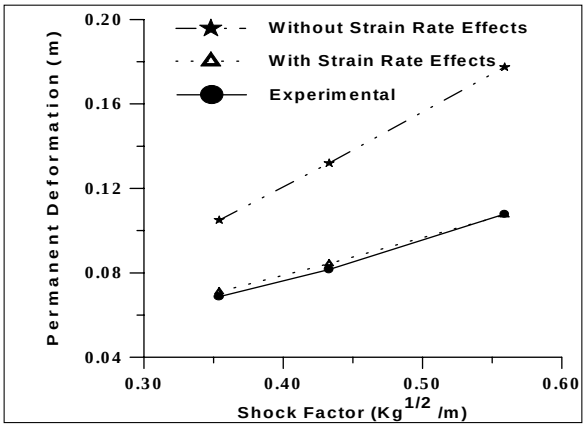

b) h/l=0.05

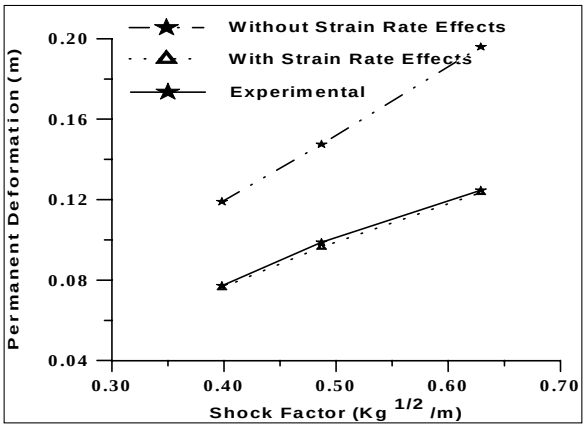

c) h/l=0.10

Fig. 13. Comparison of central (Point C in Fig. 3) permanent deformation for various shell panels.

strain rate considerably affects the dynamic response. Use of average strain rate in finite element analysis in conjunction with the Cowper – Symonds relation predicts the permanent set of the panel with engineering accuracy. Such an analysis will evidently be more economical than the one using instantaneous strain rates.

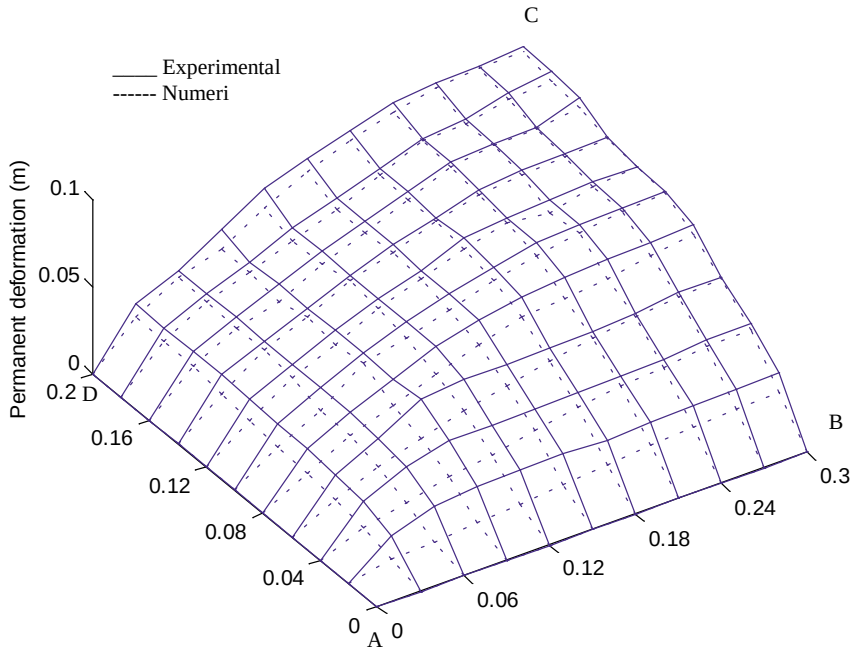

Fig. 17. Comparison of permanent deformation on a quadrant of the test panel (see Fig. 3) (Permanent deformation measured from initial panel surface towards base) ($h/l = 0.1$, Charge weight $= 30$ gm).

The membrane action of the shell panel considerably reduces the strain rate and hence, the dynamic yield compared to that of flat plates. Because of this as well as due to snap through deformation, the curved panels show larger permanent set than the flat plate. The influence of geometric imperfections and residual stresses in the curved panels needs to be investigated. The difference between numerical and experimental results may partly be due to the use of Taylor's plate theory to approximate fluid-structure interaction in the case of curved panels.

Acknowledgment

The authors are grateful to RAdm S.Mohapatra, Director, NSTL for his permission to avail the experimental facilities and publication of the work. The experimental support rendered by members of the shock studies division of NSTL is gratefully acknowledged.

References

[1] A.H. Keil, Introduction to underwater explosion research, UERD report 19–56, Norfolk naval ship yard, Portsmouth, Virginia, 1956.

[2] A.H. Keil, The response of ships to underwater explosion, *Transactions of Society of Naval Architects and Marine Engineers* **69** (1961), 360–410.

[3] A.D. Gupta, F.H. Gregory, R.L. Bitting and S. Bhattacharya, Dynamic analysis of an explosively loaded hinged rectangular plate, *Computers and Structures* **26** (1987), 339–344.

[4] R. Houlston and J.E. Slater, Damage analysis with ADINA of Naval panels subjected to a confined air blast wave, *Computers and Structures* **47** (1993), 629–639.

[5] R. Houlston, J.E. Slater, N. Pegg and C.G. DesRachers, On analysis of structural response of ship panels to air blast loading, *Computers and Structures* **21** (1985), 273–289.

[6] J. Jiang and M.D. Olson, New Design – Analysis Techniques for Blast Loaded Stiffened Box and Cylindrical Shell Structures, *International Journal of Impact Engineering* **13** (1993), 189–202.

[7] M.R. Khalil, M.D. Olson and D.L. Anderson, Non-linear Dynamic Analysis of Stiffened Plates, *Computers and Structures* **29** (1988), 929–941.

[8] T.S. Koko and M.D. Olson, Non-linear Analysis of Stiffened plates using super elements, *International Journal for Numerical Methods in Engineering* **31** (1991), 319–343.

[9] T.S. Koko and M.D. Olson, Non-linear Transient Response of Stiffened plates to Air Blast Loading by a super element Approach, *Computer Methods in Applied Mechanics and Engineering* (1991), 737–760.

[10] M.D. Olson, G.N. Nurick and J.R. Fagnan, Deformation and rupture of blast loaded square plates – predictions and Experiments, *International Journal of Impact Engineering* **13** (1993), 279–291.

[11] G.N. Nurick, M.D. Olson, J.R. Fagnan and A. Levin, Deformation and tearing of blast loaded stiffened square plates, *International Journal of Impact Engineering* **15** (1995), 273–291.

[12] M.H. Klaus, Response of a Panel Wall Subjected to Blast Loading, *Computers and Structures* **21** (1985), 129–135.
[13] L.A. Louca and J.E. Harding, Non-linear analysis of imperfect plates under transient lateral pressure loading, *Computers and Structures* **63** (1997), 27–37.
[14] Z. Qingjle, L. Shiqi and J. Zheng, Nonlinear dynamic behavior of stiffened plate under instantaneous loading, *Computers and Structures* **40** (1991), 1351–1356.
[15] T. Wierzbicki and A.L. Florence, A theoretical and experimental investigation of impulsively loaded clamped circular viscoplastic plates, *International Journal of solids and structures* **6** (1970), 553–568.
[16] G. Sinha and M. Mukhopadyay, Linear transient dynamic response of stiffened plates by the finite element method, Report No. MST/10, Department of naval Architecture, IIT, Kharagpur, India, 1992.
[17] M.V. Dharaneepathy and C.K. Madheswaran, Influence of stiffener patterns on impact response of steel panels, *IE*(*I*) *Journal-CV* (1997), 44–48.
[18] S.B. Menkes and H.J. Opat, Tearing and shear failures in explosively loaded clamped beams, *Explosion Mechanics* **13** (1973), 480–486.
[19] K. Ramajeyathilagam, C.P. Vendhan and V. Bhujanga Rao, Non-linear transient dynamic response of rectangular plates under shock loading, *International Journal of Impact Engineering* **24**(10) (2000), 999–1015.
[20] CSA/GENSA user manual, CSA Research Corporation, California, USA, 1996.
[21] T.J.R. Hughes and W.K. Liu, Nonlinear finite element analysis of shells: Part I. Three dimensional shells, *Computer methods in Applied Mechanical Engineering* **26** 331–362.
[22] N. Jones, *Structural Impact*, Cambridge University press, Cambridge, UK, 1989.
[23] R.H. Cole, *Underwater Explosions*, Dover Publications Inc, Newyork, USA, 1948.
[24] G.I. Taylor, The pressure and impulse of submarine explosion waves on plates, Compendium of Underwater Explosion Research, *ONR* **1** (1950), 1155–1174.

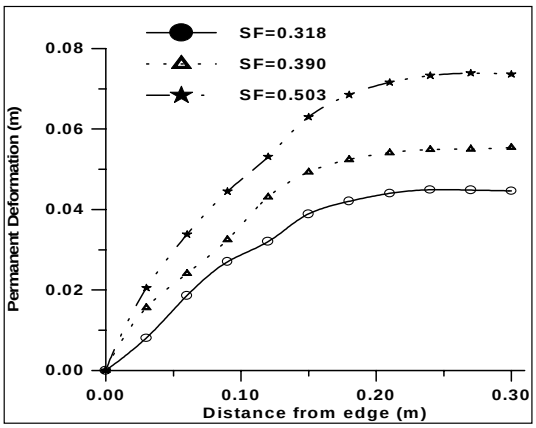

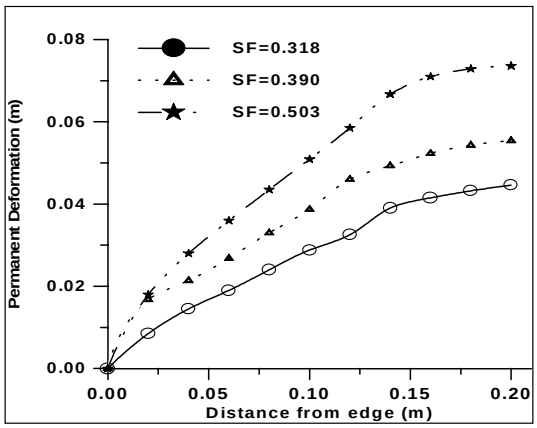

h/l=0.0

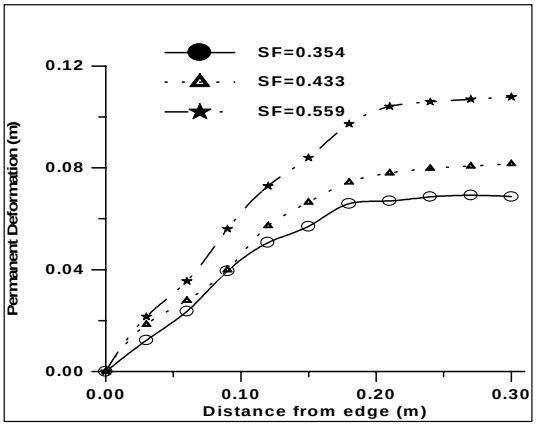

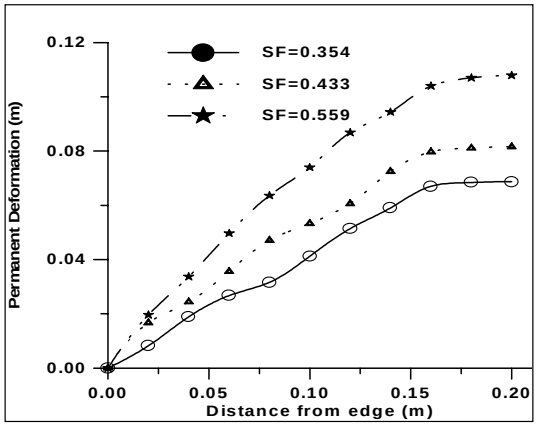

h/l=0.05

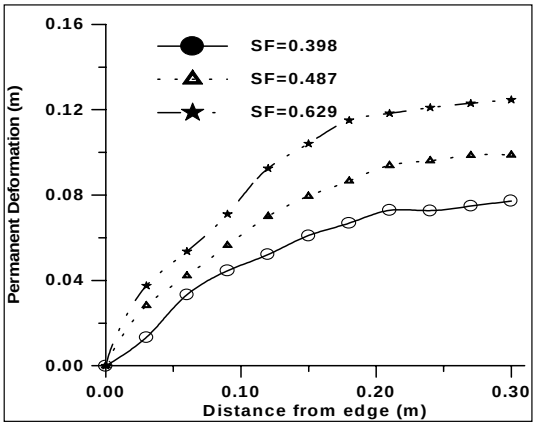

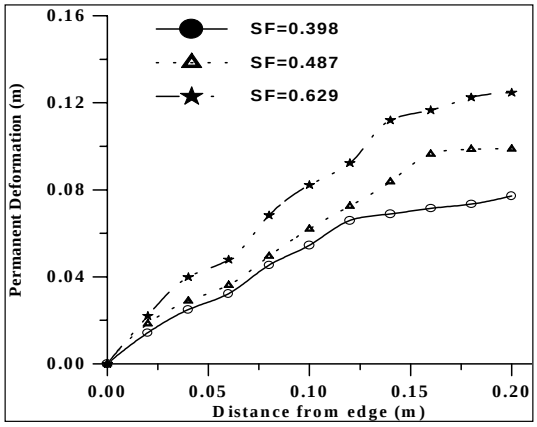

h/l=0.1

a) Longitudinal (line DC in Fig.3) b) Transverse (line BC in Fig.3)

Fig. 6. Permanent deformation of the shell panel measured from the original position (Experimental) (SF = Shock Factor).

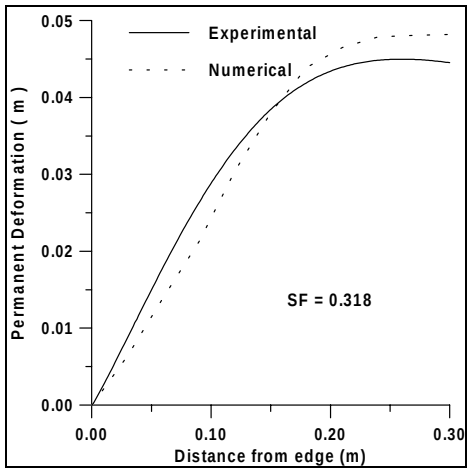

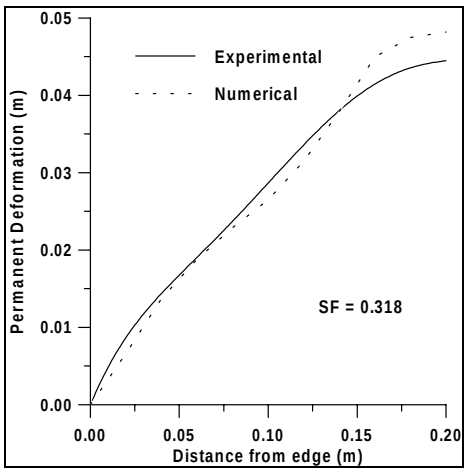

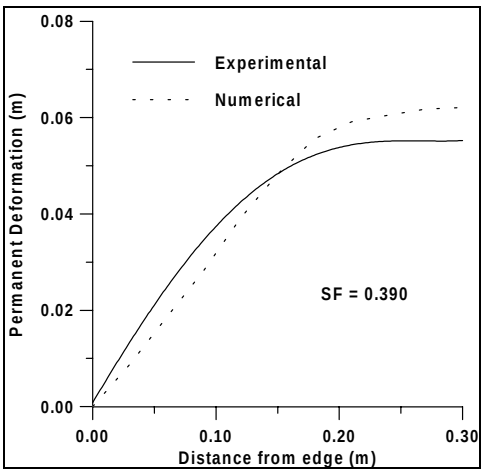

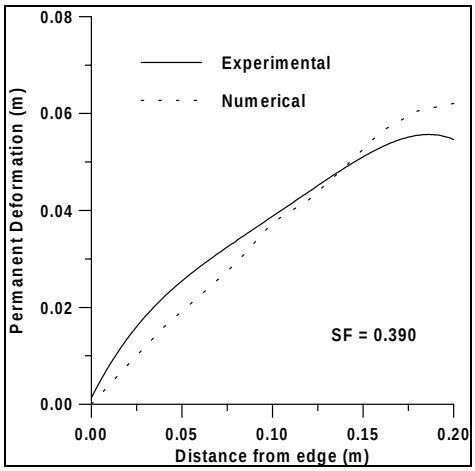

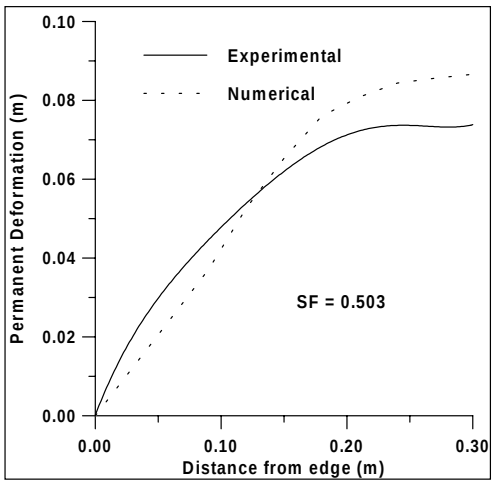

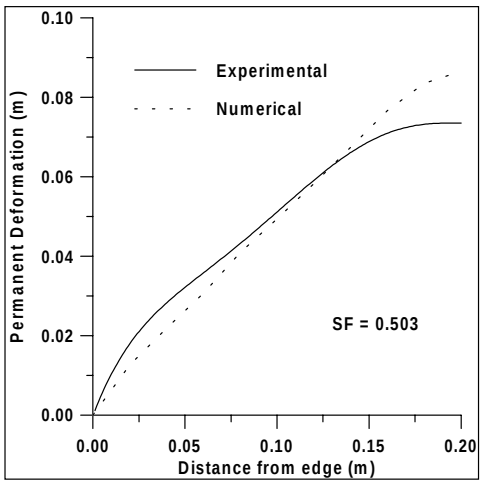

a) Longitudinal (DC in Fig. 3) b) Transverse (BC in Fig. 3)

Fig. 14. Comparison of permanent deformation along center line ($h/l = 0.0$).

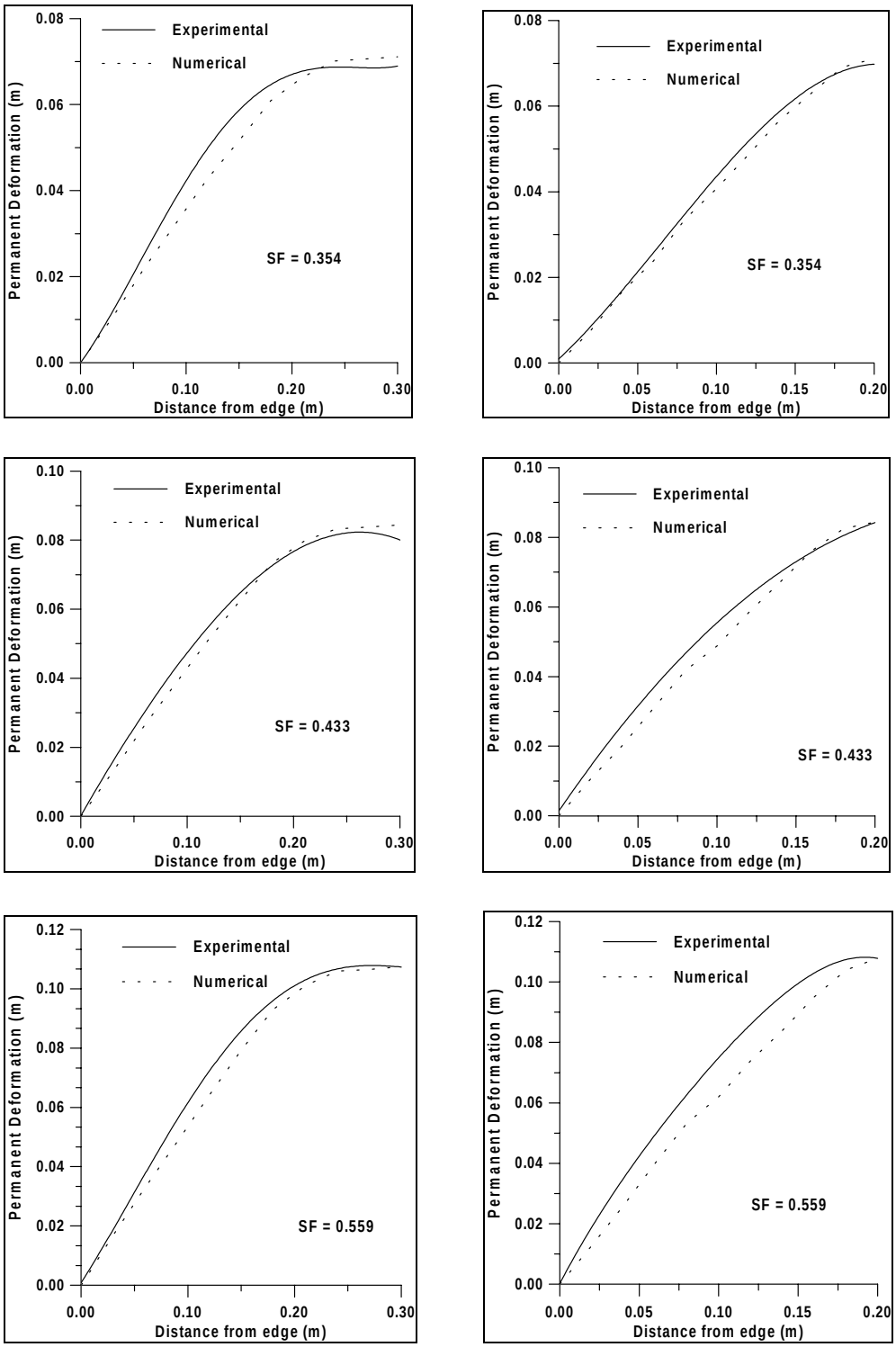

a) Longitudinal (DC in Fig. 3) b) Transverse (BC in Fig. 3)

Fig. 15. Comparison of permanent deformation along center line ($h/l = 0.05$).

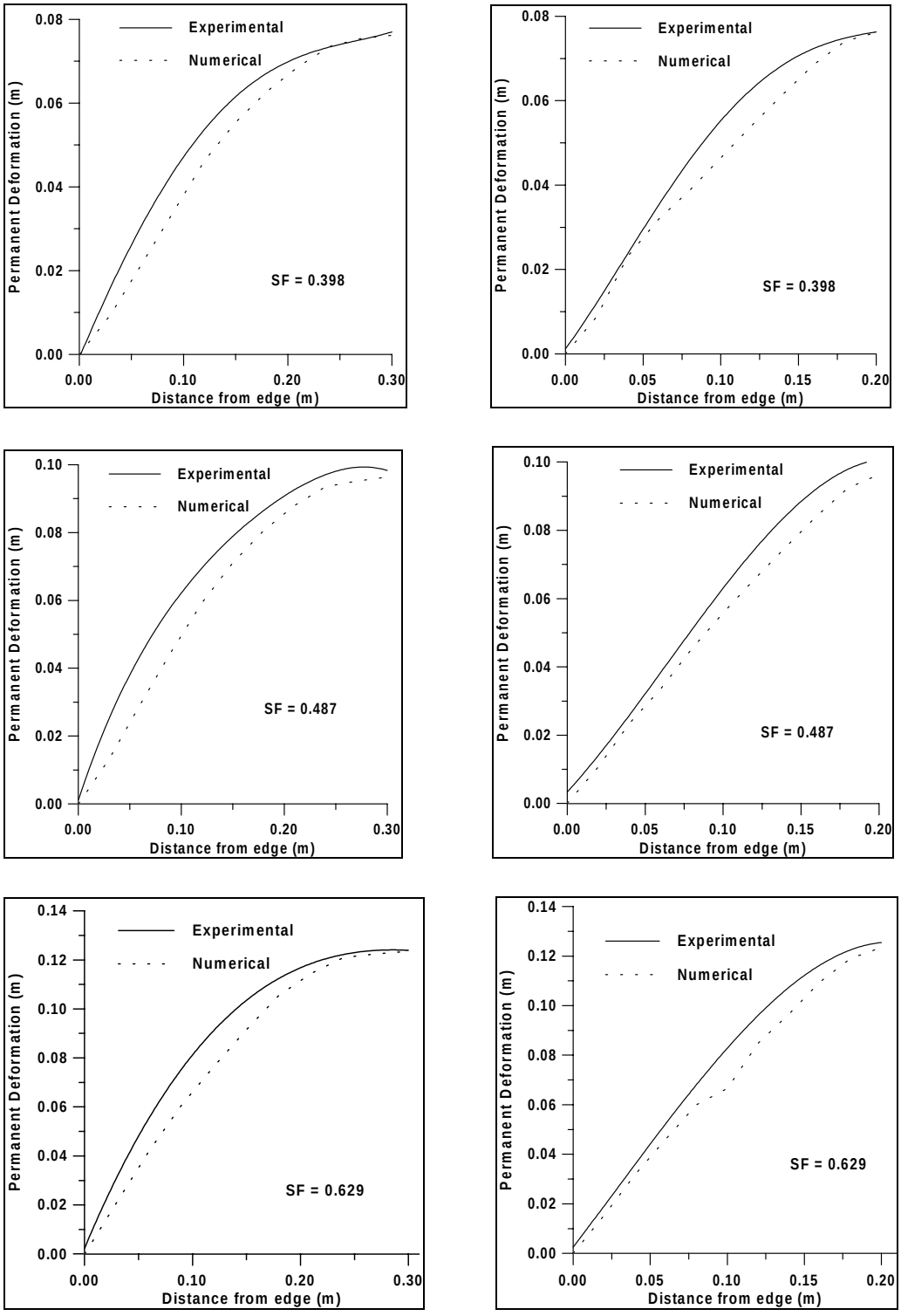

(a) Longitudinal (DC in Fig. 3) (b) Transverse (BC in Fig. 3)

Fig. 16. Comparison of permanent deformation along center line ($h/l = 0.1$).